

RESEARCH ARTICLE

 OPEN ACCESS

Received: 15-11-2021

Accepted: 08-02-2022

Published: 14.04.2022

Citation: Kurmi S, Litoriya PK, Verma A (2022) Structural Interpretation and Photoluminescence Properties of $\text{Sr}_{0.90-x}\text{Ca}_{0.10}\text{Al}_{12}\text{O}_{19}:\text{Dy}_x^{3+}$ Nanophosphors Synthesis by Combustion system. Indian Journal of Science and Technology 15(15): 649-657. <https://doi.org/10.17485/IJST/v15i15.2115>

* Corresponding author.

swatikurmi1@gmail.com

Funding: None

Competing Interests: None

Copyright: © 2022 Kurmi et al. This is an open access article distributed under the terms of the [Creative Commons Attribution License](https://creativecommons.org/licenses/by/4.0/), which permits unrestricted use, distribution, and reproduction in any medium, provided the original author and source are credited.

Published By Indian Society for Education and Environment ([iSee](https://www.isee.org/))

ISSN

Print: 0974-6846

Electronic: 0974-5645

Structural Interpretation and Photoluminescence Properties of $\text{Sr}_{0.90-x}\text{Ca}_{0.10}\text{Al}_{12}\text{O}_{19}:\text{Dy}_x^{3+}$ Nanophosphors Synthesis by Combustion system

Swati Kurmi^{1*}, Praveen Kumar Litoriya¹, Ashish Verma¹¹ Department of Physics, Dr. Harisingh Gour Central University Sagar, M.P, 470003, India

Abstract

Objectives: To synthesize a phosphor of more intense, high color purity, and to last longer. **Methods:** We have synthesized $\text{Sr}_{0.90-x}\text{Ca}_{0.10}\text{Al}_{12}\text{O}_{19}:\text{Dy}_x^{3+}$ ($x=0.00, 0.01, 0.03, 0.05, 0.07$) phosphors using a low temperature (560 ± 10) °C combustion system. X-ray diffraction, Field Emission Scanning Electron Microscopy (FE-SEM), and EDS spectra were used to perform phase identification, morphological examination, and elemental analysis. Spectroscopic photoluminescence techniques of the described phosphor were used to investigate its optical properties. **Findings:** According to scherrer's formula, the crystal size of strontium calcium aluminates phosphor is between 12.58 and 84.67 nm. The Dy^{3+} emission peaks at 475 nm (blue), 573 nm (yellow-green), and 666 nm (red) in the phosphor. PL emission spectra can be attributed to the 4f-4f transition of Dy^{3+} ions. The phosphor color purity is 15%, and the average life time is 0.96 ms, indicating that it will survive a long last. The intensity at the wavelengths of 475nm and 575 nm is 40000 counts and 35000 counts, respectively. **Novelty:** With a 0.10 molar calcium concentration, we have synthesized strontium aluminates phosphor with improved properties. The described phosphor has long-lasting applications as a refractory structural material, great and useful material for pale-orange colorants, and may be employed in many solid-state lighting technologies.

Keywords: Strontium Aluminates Phosphor; Paleorange Phosphor; Photoluminescence; Correlated Color Temperature; Combustion System

1 Introduction

Phosphor materials are utilized in Cathode Ray Tube (CRT) and plasma video display screens, fluoroscope screens, fluorescent lights, scintillation sensors, and white LEDs, as well as luminous paints⁽¹⁾. Due to their extended afterglow qualities, phosphor materials are acceptable as energy storing materials. They can absorb UV-visible light and moderately release the absorbed energy at a certain wavelength in the dark⁽²⁾. Phosphors come in a variety of forms at the moment. The earliest phosphors with Cu and Mn were made from ZnS-based compounds. They have been used in a number of

different fields. These phosphors have insufficient luminous intensity and a short afterglow period⁽³⁾. As a result, a variety of radioactive materials were used to increasing the afterglow time and some radioactive elements like Co and Pm have to be co-doped into the ZnS origin to extend the afterglow time. When compared to phosphor based on sulphide and phosphor based on oxide, phosphor based on aluminates has been discovered as a more suitable host material. Chemical stability, no radioactive radiations, environmental capabilities, and long phosphorescence persistence are all advantages of aluminates-based phosphors⁽⁴⁾. Dy³⁺ ions were commonly utilized as an activator ion for various host lattices in order to evaluate phosphor. Researchers began looking for greater luminous and long-lasting phosphors as a result of this⁽⁵⁾. The composition of Al/Sr/Ca impacts of flux, composition of rare earth ions, charge compensator ions, and heating temperature and time for SrCaAl₁₂O₁₉ phosphor have not been thoroughly investigated.

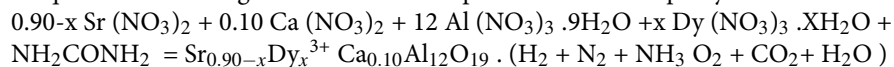
Bahram et al. created SrAl₁₂O₁₉:Pr³⁺ nanophosphors using the combustion process⁽⁶⁾. Abhay Deshmukh et al. created SrAl₁₂O₁₉:Eu³⁺ nanophosphors. Similarly, Kapil et al. created SrAl₁₂O₁₉:Dy³⁺ nanophosphors via the combustion process, with absorption peaks at 324, 350, 364, and 387 nm in visible wavelengths. When stimulated by 350 nm, two emission peaks were seen at 478 nm and 573 nm. Radioactive free long lasting persistent after glow luminescence phosphors based on SrAl₂O₄:Eu²⁺, Dy³⁺ was discovered by Japanese scientists Matsuzawa et al. in 1996 (J. Electrochem). It was a breakthrough in the field of luminescence⁽⁷⁾.

We synthesized the SrCaAl₁₂O₁₉ (host) material based on the advantages of Dy³⁺ ions, which may have a variety of useful features. As a result, we decided to investigate and study the material properties of Sr_{0.90-x}Ca_{0.10}Al₁₂O₁₉:Dy_x³⁺ (x=0.00, 0.01, 0.03, 0.05, and 0.07) in this paper.

2 Material and Methods

2.1 Synthesis of Sr_{0.90-x}Ca_{0.10}Al₁₂O₁₉:Dy_x³⁺ Phosphor

At (560 ± 10)°C, the phosphor Sr_{0.90-x}Ca_{0.10}Al₁₂O₁₉:Dy_x³⁺ (x=0.00, 0.01, 0.03, 0.05, 0.07) was synthesized using a combustion synthesis apparatus. Starting AR grade ingredients (99.99 % purity) were employed to generate phosphors, including strontium nitrate [Sr(NO₃)₂] (Merck), aluminum nitrate nine-hydrate [Al(NO₃)₃.9H₂O] (Merck), calcium nitrate tetra hydrate [Ca(NO₃)₂.4H₂O] as host lattice, dysprosium nitrate [Dy(NO₃)₃.xH₂O] as a dopant and urea (NH₂CONH₂) (Merck), was used as fuel. The oxidizer-to-fuel ratio has been set to one⁽⁸⁾. The analytical balance (WENSA) was used to weigh the appropriate number of reactants. Using an agate motor pestle, the raw components were successfully mashed into a thick paste. They were placed in a china crucible and then burnt in a vertical muffle furnace at a constant temperature of (560 ± 10)°C. At first, the mixture boils and dehydrates. After that, significant quantities of gases (oxides of carbon) are released and the process becomes exothermic, resulting in spontaneous flaming⁽⁹⁾. The solution flowed through, causing a large amount of irritation and creating white frothy ash. The flame temperature rises to a point where the vapor phase oxides are converted to mixed aluminates. The flame lasts about 20 seconds before the crucible is removed from the furnace and the frothy product is pulverized for 45 minutes at room temperature to yield a homogeneous white powder of Sr_{0.90-x}Ca_{0.10}Al₁₂O₁₉:Dy_x³⁺⁽⁶⁾. Powder materials were annealed at 1000° C for four hours in a high temperature muffle furnace to improve crystallinity. The flow diagram for the combustion technique is shown in Figure 1. The chemical process for the sample synthesis is blown out.



2.2 Phosphors Characterization Techniques

The X-ray Diffractometer was used to determine the crystal size, crystalline structure, and particle size of the predominant powdered material. Details regarding the surface structure, surface morphology, and elemental analysis, among other things, were obtained using field emission scanning electron microscopy and EDS Spectra. Transmission electron microscopy was used to examine the substance's internal structure and particle size. The purity of the material was measured using Fourier transform infrared. The excitation and emission spectra were measured using a photoluminescence spectrometer to examine PL properties.

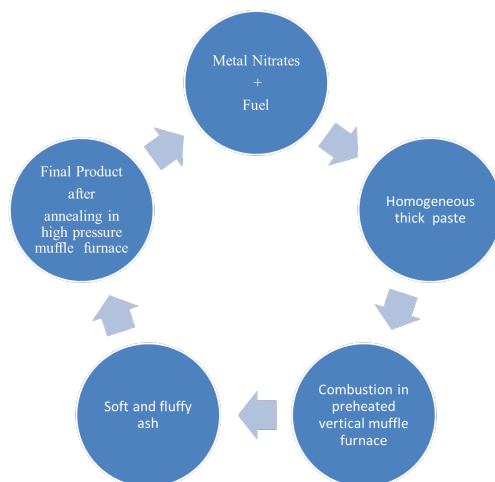


Fig 1. Flow chart for combustion system

3 Results and Discussions

3.1 Powder X-ray Diffraction (PXRD Analysis)

The diffraction peaks of $Sr_{0.90-x}Ca_{0.10}Al_{12}O_{19}:Dy_x^{3+}$ ($x=0.00, 0.01, 0.03, 0.05, 0.07$) phosphor synthesized through combustion synthesis system are shown in the X-ray diffraction pattern Figure 2a. Because the level of impurity doping is minimal, the XRD peaks of doped and undoped are identical. All of the samples XRD patterns are shown in Figure 2a and match the typical XRD pattern of $SrAl_{12}O_{19}$ (JCPDS File No. 89-2505)⁽¹⁰⁾. The crystalline properties of the material formed by the sharpness of the peaks are well demonstrated, as well as the particle size being nano due to some peak broadening. The XRD diffraction peaks of the hexagonal phase are idiosyncratic to the [101], [102], [006], [110], [107], [114], [203], [204], [205], [1010], [303], [304], [215], [2014], and [1016] lattice planes of hexagonal phase (P6₃/mmc). Crystal parameters ($a = b \neq c$) and crystal volume are computed using (Eq.1), where a, b, and c are crystal parameters, and d_{hkl} is the interplanar spacing corresponding to the miller indices h, k, and l in Table 1.

$$\frac{1}{d_{hkl}^2} = \frac{h^2}{a^2} + \frac{k^2}{b^2} + \frac{l^2}{c^2} \text{ [Eq.1]; } D = \frac{K\lambda}{\beta \cos \theta} \text{ [Eq. 2] ; } 2d \sin \theta = n \lambda \text{ [Eq.3] ; } \epsilon = \frac{\beta}{4 \tan \theta} \text{ [Eq. 4]}$$

The crystallite size and crystal strain of the samples are calculated by the Scherer formula (Eq .2) and hall Williamson equation (Eq.4) respectively, as shown in Table 2⁽¹¹⁾. The crystalline size were found to be in the range of 12.58 nm – 84.67 nm of synthesized phosphor. The low crystal strain and high crystalline properties are due to peak sharpness. The main reason for peak sharpness is urea (NH₂CONH₂) which increases the temperature of combustion to high temperature⁽¹⁰⁾. By these crystalline properties of synthesized phosphor increased. When we have intentionally introducing impurities (in sufficient amount) to the host phosphors, the lattice parameters of the crystal will dilate giving rise to a slight shift in the peaks at the direction of higher angle. The results obtained are displayed in Figure 2b. The data of crystal parameters and volume of lattice cell is tabulated in Table 1. The Sample name, average crystal size, FWHM and calculated crystallite strain of the synthesized powder sample also tabulated in Table ??.

Table 1. Lattice parameter and Cell Volume for $Sr_{0.90-x}Ca_{0.10}Al_{12}O_{19}:Dy_x^{3+}$ ($x=0.00, 0.01, 0.03, 0.05, 0.07$)

Samples	lattice Parameter ($a = b \neq c$)		Cell Volume
	a (Å)	c (Å)	
SrCaAl12O19:Dy3+0.00	4.79	19.01	438.23
SrCaAl12O19:Dy3+0.01	4.71	21.80	483.61
SrCaAl12O19:Dy3+0.03	4.78	21.63	494.21
SrCaAl12O19:Dy3+0.05	4.80	21.86	503.65
SrCaAl12O19:Dy3+0.07	4.83	22.00	513.23

Table 2. FWHM values, crystal size, d-spacing and Miller indices for $\text{Sr}_{0.90-x}\text{Ca}_{0.10}\text{Al}_{12}\text{O}_{19}:\text{Dy}^{3+}_x$ ($x=0.00, 0.01, 0.03, 0.05, 0.07$).

Samples	2θ (degree)	FWHM (degree)	Crystal Size (nm)	Micro Strain	d-Spacing (nm)	Miller Indices (hkl)
SrCaAl ₁₂ O ₁₉ :Dy ³⁺ +0.00	49.66	0.29	12.58 72.66	0.03	0.18	[1011]
SrCaAl ₁₂ O ₁₉ :Dy ³⁺ +0.01	67.33	0.17	39.47 84.67	0.02	0.14	[1015]
SrCaAl ₁₂ O ₁₉ :Dy ³⁺ +0.03	36.44	0.14	38.79 72.66	0.10	0.25	[200]
SrCaAl ₁₂ O ₁₉ :Dy ³⁺ +0.05	60.30	0.24	32.4078.48	0.03	0.15	[2011]
SrCaAl ₁₂ O ₁₉ :Dy ³⁺ +0.07	71.88	0.45	27.27 74.45	0.08	0.13	[315]

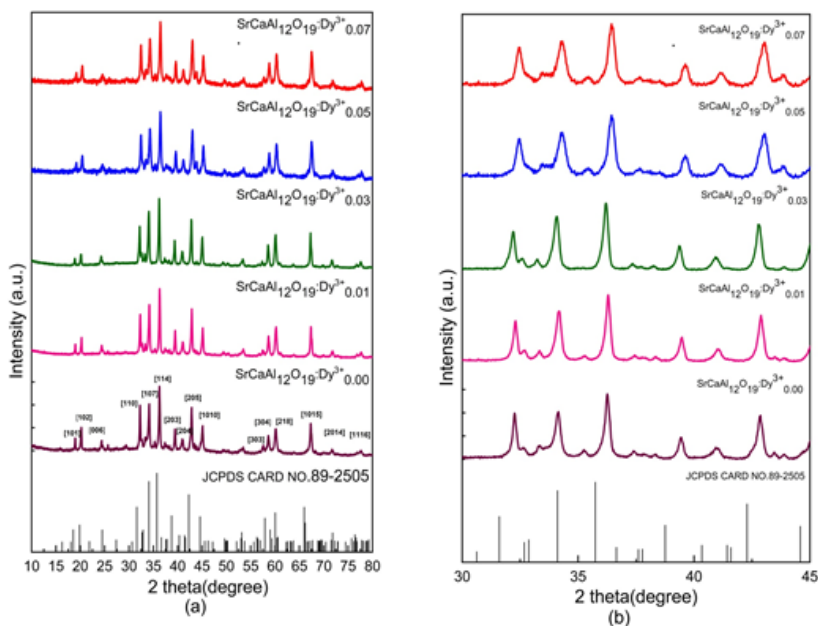


Fig 2. (a) Theoretical and experimental PXRD pattern of $\text{Sr}_{0.90-x}\text{Ca}_{0.10}\text{Al}_{12}\text{O}_{19}:\text{Dy}^{3+}_x$ ($x=0.00, 0.01, 0.03, 0.05, 0.07$) (b) Extended view of main peak of PXRD pattern

3.2 Scanning Electron Microscopy and EDS Analysis

The morphology and microstructure of synthesized nanoparticles were studied using SEM data from several samples. The foamy, non-uniform forms and agglomerated character of the powder samples were clearly visible in the SEM images presented in Figure 3. The EDS spectrum was used to determine the elemental compositions of the synthesized phosphors, which are shown in Table 3. The Dy-doped $\text{SrCaAl}_{12}\text{O}_{19}$ phosphor shows peaks of strontium (Sr), aluminum (Al), oxygen (O), and dysprosium (Dy) elements, as shown in Figure 4 (a-d). As a result, the EDS data show that Dy^{3+} ions have been well integrated into the $\text{SrCaAl}_{12}\text{O}_{19}$ host⁽¹²⁾.

3.3 Transmission Electron Microscopy (TEM Analysis)

TEM was used to examine the size and structure of nanoparticles in greater detail. TEM images of $\text{Sr}_{0.90-x}\text{Ca}_{0.10}\text{Al}_{12}\text{O}_{19}:\text{Dy}^{3+}_x$ ($x = 0.07$ % molar concentration) nanoparticles with particle sizes ranging from 14 to 30 nm are shown in Figure 5. The considerable variance in particle size could be due to agglomeration. We can plainly observe from the TEM image that the particles are precisely hexagonal, but deformed hexagonal. The doping of Dy-ions atoms in the hexagonal lattice of $\text{SrCaAl}_{12}\text{O}_{19}$ causes this deformation in particle shape. The computed d-spacing from the HRTEM image is 1.12 nm, 0.58 nm, and 0.38 nm. We can see that there are white spots surrounding the core bright area and some ring in the SAED pattern

Table 3. Tabulation of element distribution of $\text{Sr}_{0.90-x}\text{Ca}_{0.10}\text{Al}_{12}\text{O}_{19}:\text{Dy}_x^{3+}$ ($x=0.03$).

Element	Weight %	Atomic %	Net Int.	Error %	P/B Ratio	R	F
Oxygen K-Series	45.56	63.49	96.99	18.23	0.0000	1.0000	1.0000
Aluminum K-Series	40.22	33.23	455.00	14.86	343.7694	1.0092	1.0032
Srtrium L-Series	6.93	1.76	27.35	27.03	50.7908	1.0125	1.0013
Calcium K-Series	1.21	0.68	6.63	69.06	16.8702	1.0247	1.0269
Dysprosium L-series	6.08	0.83	3.02	74.51	56.4136	1.0343	1.0216

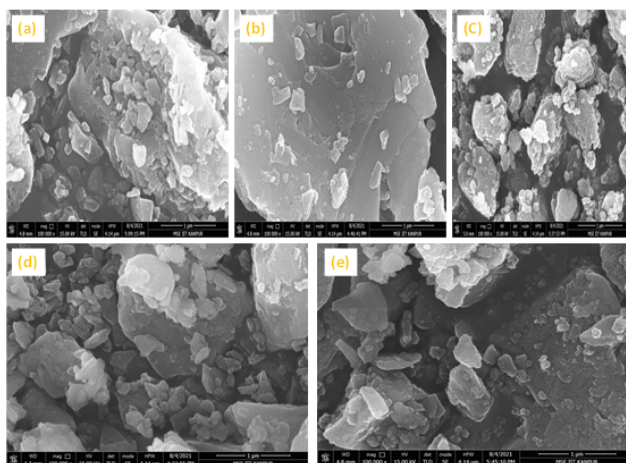


Fig 3. (a - e). SEM image of $\text{Sr}_{0.90-x}\text{Ca}_{0.10}\text{Al}_{12}\text{O}_{19}:\text{Dy}_x^{3+}$ ($x=0.00, 0.01, 0.03, 0.05, 0.07$)

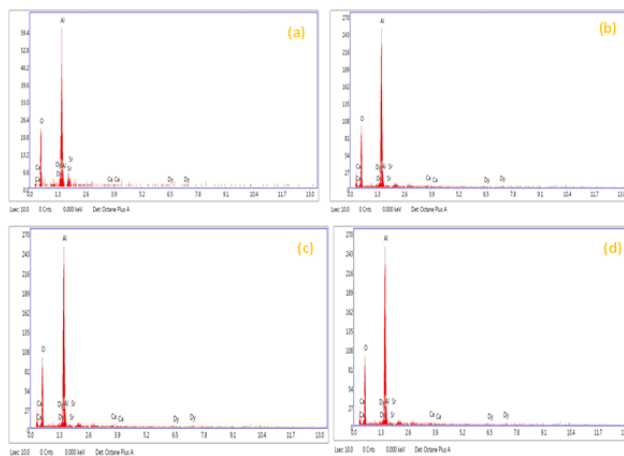


Fig 4. EDS spectra of $\text{Sr}_{0.90-x}\text{Ca}_{0.10}\text{Al}_{12}\text{O}_{19}:\text{Dy}_x^{3+}$ ($x=0.01, 0.03, 0.05, 0.07$)

Figure 4d. This demonstrates that samples contain big particles⁽¹³⁾. Image-j software was used to calculate D-values for the [002], [004], [103], and [102] planes. These values are determined to be consistent with the XRD results for these planes.

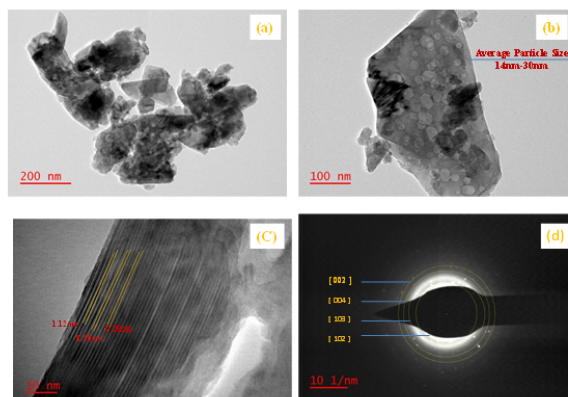


Fig 5. (a) & (b) TEM image of $\text{SrAl}_{12}\text{O}_{19}:\text{Dy}^{3+}_{0.07}$ sample referring particle size distribution in nm range (c) The HRTEM image of sample exposition the lattice fringes (d) The SAED pattern of sample, labeled with lattice planes.

Table 4. d-spacing and hkl values for $\text{SrCaAl}_{12}\text{O}_{19}:\text{Dy}^{3+}_{0.07}$.

Sr No.	1/D (nm)	1/r (nm)	r (nm)	d-Spacing (Å)	hkl value
1	17.06	8.53	0.117	1.27	002
2	38.34	19.17	0.052	0.52	004
3	43.03	21.51	0.046	0.46	102
4	46.50	23.25	0.043	0.43	103

3.4 FTIR Analysis

The absorption peaks of $\text{Sr}_{0.90-x}\text{CaAl}_{12}\text{O}_{19}\text{Dy}_x^{3+}$ ($x = 0.00, 0.01, 0.03, 0.05, 0.07$) in the 500 cm^{-1} to 4000 cm^{-1} range, as illustrated in Figure 6. The FTIR spectra are made up of absorption peaks derived from FTIR spectroscopic data in order to identify active functional groups, organic–inorganic impurities, and symmetric and anti-symmetric stretching between active bands. At 2363 cm^{-1} , the peaks can be attributable to ambient water vapour. These peaks are responsible for the ant symmetric stretching vibrations of unbound O - H bonds. C - O vibrations could account for the peaks found at 760 cm^{-1} . The residual carbon in the samples or CO_2 absorption from the surroundings could be the cause of these peaks. Al-O vibrations account for the peak at 689 cm^{-1} , while Sr-O vibrations account for the peak at 579 cm^{-1} . As a result, the peaks detected in the IR range between 800 cm^{-1} and 500 cm^{-1} can be attributed to the typical metal-oxygen (M -O) vibrations, indicating the creation of $\text{SrCaAl}_{12}\text{O}_{19}$ crystals⁽¹⁴⁾.

3.5 Photoluminescence (PL Analysis)

The excitation and emission spectra of the synthesized phosphor $\text{Sr}_{0.90-x}\text{Ca}_{0.10}\text{Al}_{12}\text{O}_{19}:\text{Dy}_x^{3+}$ ($x = 0.00, 0.01, 0.03, 0.05, 0.07$) were noticed and exhibited in the study of luminescence properties Figure 7. The phosphor was excited with 470 nm radiations in the excitation spectra, and the excitation spectra were collected over a range of 320 nm to 440 , and the emission spectra were collected over a range of 450 nm to 680 nm . Dy^{3+} ions are excited from their ground state ${}^6\text{H}_{15/2}$ to a variety of excited states, resulting in a variety of excitation peaks in the UV and visible spectrum. The first peak was detected at 350 nm (${}^6\text{H}_{15/2}-{}^6\text{P}_{7/2}$), the second peak at 364 nm (${}^6\text{H}_{15/2}-{}^6\text{P}_{5/2}$), the third peak at 387 nm (${}^6\text{H}_{15/2}-{}^4\text{I}_{13/2}$) and the fourth peak at 427 nm in excitation spectra. In the emission spectra, three height peaks were found at 475 nm , 573 nm , and 666 nm ⁽¹⁵⁾. All emissions occur through excitations within Dy^{3+} through 4f-4f forbidden transitions which are usually quite weak compared to 4f-5d allowed transitions from Eu^{2+} or Ce^{3+} because of which the latter two ions are employed in most lighting devices⁽¹⁾⁽¹⁶⁾. Maximum intensity in emission spectra is found for $\text{Dy}^{3+}(0.07)$ in the pale-orange area. At a wavelength of 350 nm , the decay curve and average life

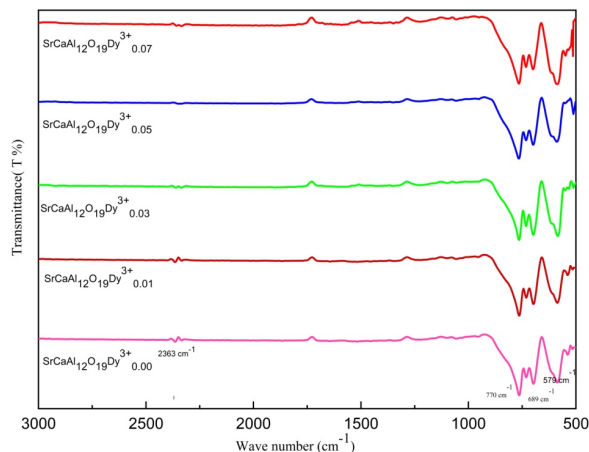


Fig 6. FTIR spectra of $\text{Sr}_{0.90-x}\text{Ca}_{0.10}\text{Al}_{12}\text{O}_{19}:\text{Dy}_x^{3+}$ ($x=0.00, 0.01, 0.03, 0.05, 0.07$).

duration of $\text{Sr}_{0.90-x}\text{Ca}_{0.10}\text{Al}_{12}\text{O}_{19}:\text{Dy}_x^{3+}$ phosphors ($x = 0.01, 0.03, 0.05$, and 0.07) are shown in Figure 8. It indicates that curve could be well fitted in single exponential decay function.

3.5.1 Chromaticity Co-ordinate and Correlated Color Temperature

International Commission of l'Eclairage to investigate the emission color of synthesized phosphors, a chromaticity co-ordinates (1931) diagram was displayed in Figure 9 Using PL emission spectra, the chromaticity co-ordinates of synthesized phosphors were estimated and displayed in a 1931 chromaticity co-ordinate diagram with unique dopant concentrations, as shown in.

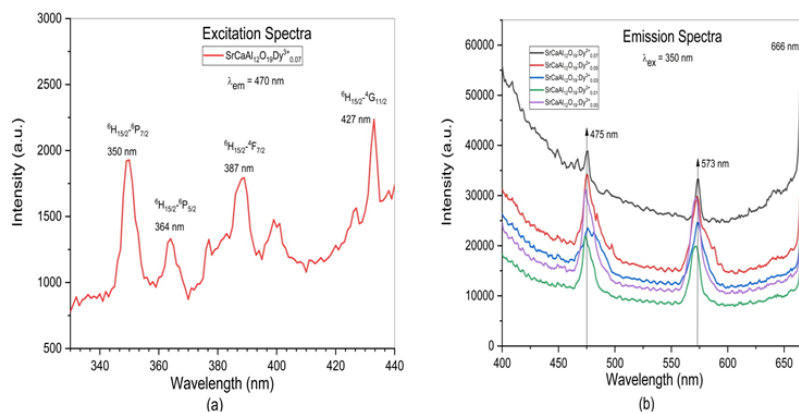


Fig 7. (a) Photoluminescence excitation spectra of $\text{Sr}_{0.90-x}\text{Ca}_{0.10}\text{Al}_{12}\text{O}_{19}:\text{Dy}_{0.07}^{3+}$ (b) Photoluminescence emission spectra of $\text{Sr}_{0.90-x}\text{Ca}_{0.10}\text{Al}_{12}\text{O}_{19}:\text{Dy}_x^{3+}$ ($x=0.00, 0.01, 0.03, 0.05, 0.07$)

It was concluded from the graphic that the (x, y) co-ordinate for all dopant concentrations is in the bluish white zone. The phosphors that have been synthesized can be used to generate near-white light. Table 5 shows the calculated CIE co-ordinates of all phosphors. Color purity describes the purity of radiated light; lower color purity indicates a greater likelihood of emitting white light, whilst higher color purity indicates the creation of a specific color. It is clear that the Dy^{3+} doped $\text{SrCaAl}_{12}\text{O}_{19}$ phosphor material is an excellent cool white light source that might be used commercially for communal lighting, nUV- LED, reading lamps, and illuminating living areas⁽¹⁷⁾. The color purity of $\text{Sr}_{0.90-x}\text{Ca}_{0.10}\text{Al}_{12}\text{O}_{19}:\text{Dy}_x^{3+}$ ($x = 0.00, 0.01, 0.03, 0.05, 0.07$) phosphors was calculated using CIE chromaticity co-ordinates.

$$\text{Color purity} = \frac{\sqrt{[(x_s - x_i)^2 + (y_s - y_i)^2]}}{\sqrt{[(x_d - x_i)^2 + (y_d - y_i)^2]}} \times 100 \% \text{ [Eq.5]}$$

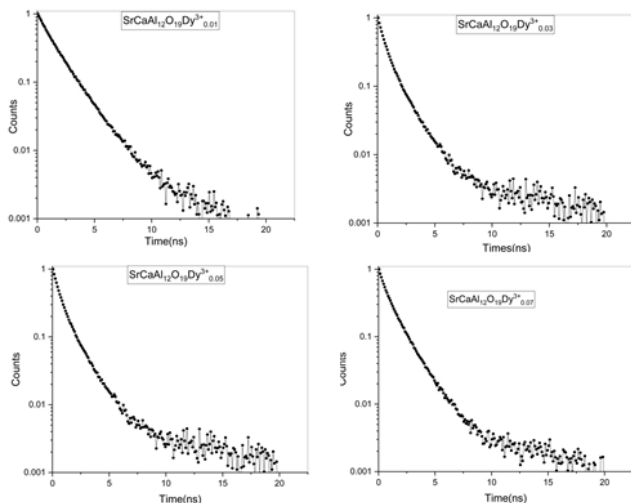


Fig 8. Decay Curve for $Sr_{0.90-x}Ca_{0.10}Al_{12}O_{19}:Dy_x^{3+}$ ($x=0.01, 0.03, 0.05, 0.07$)

Where (x_s, y_s) are the co-ordinates of phosphors reported in present work, (x_i, y_i) co-ordinates of white light and (x_d, y_d) co-ordinates of dominant wavelength. Calculated color purity of prepared phosphors is listed in Table 5.

Table 5. Average life time, correlated coordinates of chromacity (x,y) and correlated temperature (CCT) , Color purity , Quantum efficiency for $Sr_{0.90-x}Ca_{0.10}Al_{12}O_{19}:Dy_x^{3+}$ ($x = 0.01, 0.03, 0.05, 0.07$)

Sr no	Dy3+ Concentration	Average Life Time (n.s)	Color coordinate		CCT (K)	Color Purity
			X	Y		
1	0.01	0.87	0.305	0.290	7130	18 %
2	0.03	1.60	0.309	0.301	6975	16 %
3	0.05	1.15	0.310	0.305	6975	14 %
4	0.07	0.95	0.312	0.301	6975	15 %

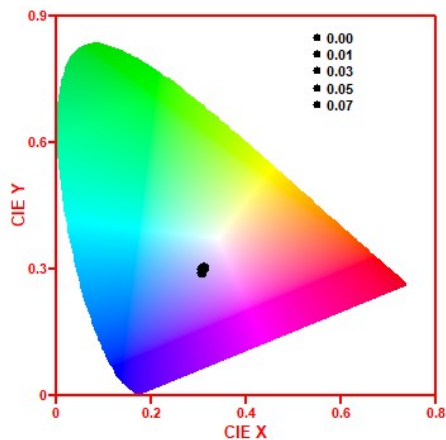


Fig 9. CIE Spectra for $Sr_{0.90-x}Ca_{0.10}Al_{12}O_{19}:Dy_x^{3+}$ ($x=0.00, 0.01, 0.03, 0.05, 0.07$)

4 Conclusion

The samples were synthesized by combustion synthesis system and annealed at 1000 °C. Sample shows hexagonal structure and the crystal size calculated by Scherer's formula ranging from 12.58 - 84.67 nm. The good connectivity with grains and the hexagonal structure was found by SEM. The study of the photoluminescence characteristics of Dy³⁺ activated pale-orange emitting SrCaAl₁₂O₁₉: Dy³⁺ phosphors in the near UV-vis and visible range show the excitation bands at 350nm -433 nm. Emission characteristics of SrCaAl₁₂O₁₉: Dy³⁺ shows emission band at 475nm – 666 nm because of the corresponding energy level. The influence of activator concentration level on the photoluminescence properties of SrCaAl₁₂O₁₉: Dy³⁺ phosphor realize in conditions of smaller changes in relativistic intensity variation of the 4f-4f transition ascribed to conceit and improved splitting of crystallographic field. The synthesized phosphors have long-lasting applications prospective pale - orange application for the solid state lighting, may be used in fluorescent lamp in photocopiers and other devices. In future by little quantity of silicon switching the aluminum can enlarge the intensity of prepared phosphor.

References

- 1) Bedyal AK, Kunti AK, Kumar V, Swart HC. Effects of cationic substitution on the luminescence behavior of Dy³⁺ doped orthophosphate phosphor. *Journal of Alloys and Compounds*. 2019;806:1127–1137. Available from: <https://dx.doi.org/10.1016/j.jallcom.2019.07.305>.
- 2) Kamboj AK, Jindal P, Verma P. Machine learning-based physical layer security: techniques, open challenges, and applications. *Wireless Networks*. 2021;27(8):5351–5383. Available from: <https://dx.doi.org/10.1007/s11276-021-02781-1>.
- 3) Awotunde JB, Chakraborty C, Adeniyi AE. Intrusion Detection in Industrial Internet of Things Network-Based on Deep Learning Model with Rule-Based Feature Selection. *Wireless Communications and Mobile Computing*. 2021;2021:1–17. Available from: <https://dx.doi.org/10.1155/2021/7154587>.
- 4) Verma A, Verma A, Bramhe GV. Shifting and enhanced photoluminescence performance of the Sr_{1-x}EuxMgAl₁₀O₁₇ phosphor. *Journal of Alloys and Compounds*. 2019;774:1168–1180. Available from: <https://dx.doi.org/10.1016/j.jallcom.2018.09.166>.
- 5) Verma A, Verma A, Bramhe GV, Sahu IP. Optical studies of the Ba_{1-x}MgAl₁₀O₁₇:Eux phosphors synthesis by combustion route. *Journal of Alloys and Compounds*. 2018;769:831–842. Available from: <https://dx.doi.org/10.1016/j.jallcom.2018.07.371>.
- 6) Pathak SK, Verma AK, Sahu IP. Photo and Mechano - luminescence properties of novel Zn_{1-x}EuxAl_{2-y}BayO₄ advance blue phosphor. *Physica condensed matter*. 2020;602(8). Available from: <https://doi.org/10.1016/j.physb.2020.412612>.
- 7) Matsuzawa T, Aoki Y, Takeuchi N, Murayama Y. A New Long Phosphorescent Phosphor with High Brightness, SrAl₂O₄:Eu²⁺,Dy³⁺. *Journal of The Electrochemical Society*. 1996;143(8):2670–2673. Available from: <https://dx.doi.org/10.1149/1.1837067>.
- 8) Patil KC, Aruna ST, Ekambaram S. Combustion Synthesis. *Current opinion in solid state and material science*. 1997;2:80060–80065. Available from: [https://doi.org/10.1016/S1359-0286\(97\)80060-5](https://doi.org/10.1016/S1359-0286(97)80060-5).
- 9) Verma A, Verma A, Panda M. Mechano-luminescence studies of nano ZnMgAl₁₀O₁₇:Eu phosphor under UV irradiation. In: and others, editor. AIP Conference Proceedings;vol. 1953. Author(s). 2018. Available from: <https://doi.org/10.1016/j.jallcom.2018.06.023>.
- 10) Verma A, Pathak SK, Verma A, Bramhe GV, Sahu IP. Tuning of luminescent properties of Zn_{1-x}MgAl₁₀O₁₇:Eux nano phosphor. *Journal of Alloys and Compounds*. 2018;764:1021–1032. Available from: <https://dx.doi.org/10.1016/j.jallcom.2018.06.023>.
- 11) Sharma P, Jain S, Gupta S, Chamola V. Role of machine learning and deep learning in securing 5G-driven industrial IoT applications. *Ad Hoc Networks*. 2021;123:102685–102685. Available from: <https://dx.doi.org/10.1016/j.adhoc.2021.102685>.
- 12) Bansal M, Goyal A, Choudhary A. Industrial Internet of Things (IIoT): A Vivid Perspective. In: Inventive Systems and Control. Springer Singapore. 2021;p. 939–949. Available from: https://doi.org/10.1007/978-981-16-1395-1_68.
- 13) Zhang X, Hou H, Fang Z, Wang Z. Industrial Internet Federated Learning Driven by IoT Equipment ID and Blockchain. *Wireless Communications and Mobile Computing*. 2021;2021:1–9. Available from: <https://dx.doi.org/10.1155/2021/7705843>.
- 14) Dev K, Selot A, Nair GB, Mehare CM, Haque FZ, Aynyas M, et al. Dhoble Synthesis and photoluminescence study of Dy³⁺ activated SrAl₁₂O₁₉ phosphor. *Optic - International Journal for Light and Electron Optics*. 2019;194. Available from: <https://doi.org/10.1016/j-ijleo.2019.163051>.
- 15) Ahmed KI, Tahir M, Habaebi MH, Lau SL, Ahad A. Machine Learning for Authentication and Authorization in IoT: Taxonomy, Challenges and Future Research Direction. *Sensors*. 2021;21(15):5122–5122. Available from: <https://dx.doi.org/10.3390/s21155122>.
- 16) Revannasiddappa GR, Basavaraj RB, Rudresha MS, Nagaraju G, Kumar S, Sasidhar N. White-light emitting Ca₂MgSi₂O₇:Dy³⁺ nanopowders: Structural, spectroscopic investigations and advanced forensic applications. *Vacuum*. 2021;184:109940–109940. Available from: <https://dx.doi.org/10.1016/j.vacuum.2020.109940>.
- 17) Junio JB, Chirawatkul P, Conato MT, Mercado CC. Substitution of Ca²⁺ in Calcite by Sn²⁺ and Sr²⁺ cations through ion exchange characterized by X-ray absorption and photoelectron spectroscopies. *MRS Advances*. 2021;6(12):342–349. Available from: <https://dx.doi.org/10.1557/s43580-021-00061-w>.